A novel in vitro tubular model to recapitulate features of distal airways: the bronchioid

Elise Maurat[1,2,*], Katharina Raasch[1,2,*], Alexander M. Leipold[3], Pauline Henrot[1,2,4], Maeva Zysman[1,2,4], Renaud Prevel[1,2,4], Thomas Trian[1,2], Tobias Krammer[3], Vanessa Bergeron[5], Matthieu Thumerel[1,2,4], Pierre Nassoy[6], Patrick Berger[1,2,4], Antoine-Emmanuel Saliba[3,7], Laetitia Andrique[5], Gaëlle Recher[6], Isabelle Dupin[1,2,8]

[1]Univ-Bordeaux, Centre de Recherche Cardio-thoracique de Bordeaux, U1045, CIC1401, Pessac, France. [2]INSERM, Centre de Recherche Cardio-thoracique de Bordeaux, U1045, CIC1401, Pessac, France. [3]Helmholtz Institute for RNA-based Infection Research (HIRI), Helmholtz-Center for Infection Research (HZI), Würzburg, Germany, [4]CHU de Bordeaux, Service d'exploration fonctionnelle respiratoire, Service de réanimation, Service de chirurgie thoracique, France. [5]VoxCell Facility, TBMcore UAR CNRS 3427, INSERM US 005, Univ-Bordeaux, France. [6]Laboratoire Photonique, Numérique et Nanosciences, UMR 5298 CNRS, Univ-Bordeaux, France. [7]University of Würzburg, Faculty of Medicine, Institute of Molecular Infection Biology (IMIB), Würzburg, Germany. [8]Institut universitaire de France (IUF).

[*] equal contribution (co-1st author)

Corresponding author: Prof. Isabelle Dupin, isabelle.dupin@u-bordeaux.fr

Centre de Recherche Cardio-thoracique de Bordeaux, INSERM U1045, 33600 Pessac, FRANCE

Tel : +33 5 47 30 27 51

"Take home" message:

A novel tubular engineered lung model called "bronchioid" shows mucociliary function and is compatible with air-liquid interface establishment.

Authors contributions:

- conception and design (PN, GR, ID)
- data acquisition (EM, KR, VB, LA, AML, TK, AES, GR)
- data analysis (EM, KR, AML, AES, ID)
- data interpretation (EM, KR, AML, PH, MZ, RP, TT, LA, PB, PN, AES, GR, ID)
- resources (PH, TT, MT, MZ, PB)
- drafting the manuscript (EM, KR, ID)
- revision and approval of the final version (All)

Conflict-of-interest statement:

Regarding conflict of interest, ID and PB has 2 patents delivered (EP N°3050574 and EP N°20173595). ID, PH and MZ report grants from the "Fondation Bordeaux Université". MZ reports personal fees from AstraZeneca, Boehringer Ingelheim, CSL Behring, Novartis, Chiesi, GlaxoSmithKline and non-financial support Lilly. PB reports grants and personal fees from Novartis, personal fees and non-financial support from Chiesi, Boehringer Ingelheim, AstraZeneca and Sanofi, personal fees from Menarini and TEVA, outside the submitted work. All other authors declare they have no competing interests.

Abstract

Background: Airflow limitation is the hallmark of obstructive pulmonary diseases. While numerous *in vitro* airway models already exist, chronic obstructives diseases currently lack an 3D culture system enabling to unveil the developmental processes underlying airway remodelling and the associated constrictive limitation. Here, we aimed to engineer a model of small airways, which would overcome the limitations of current culture systems.

Methods: Working with the Cellular Capsule Technology, we developed a so-called bronchioid model, using an innovative tubular cell-based assay and human bronchial adult stem cells derived from clinical samples.

Results: We produced a tubular scaffold made of alginate gel, that drives the spontaneous self-organisation of epithelial cells. Fine control of the level of contraction is required to obtain a model of distal bronchiole, with physiologically relevant shape and size. 3D imaging, gene expression and single-cell RNA-seq analysis of bronchioids made of bronchial epithelial cells demonstrates the tubular organization, the formation of epithelial junctions, as well as differentiation into ciliated and goblet cells. Ciliary beating is observed, at a decreased frequency in bronchioids made of cells from COPD patients. The bronchioid can be infected by rhinovirus. An air-liquid interface is introduced, that modulates gene expression.

Conclusion: We provide here a proof of concept of a perfusable bronchioid, with proper mucociliary and contractile functions. Key advantages of our approach, such as the air-liquid interface, the lumen accessibility, the recapitulation of pathological features and possible assessment of clinically pertinent endpoints, will make our pulmonary organoid-like model a powerful tool for pre-clinical studies.

Number of words in the abstract: 249

Key words: lung organoid, bioengineering, adult epithelial stem cells, differentiation, COPD, asthma

Abbreviations

ALI	Air-liquid interface
APC	Allophycocyanin
AS	Alginate solution
BEC	Bronchial epithelial cell
CCS	Core cell suspension
COPD	Chronic Obstructive Pulmonary Disease
J3B1A	EpH4-J3B1A mammary gland epithelial cell line
EDTA	Ethylene Diamine Tetra-acetic Acid
FEV_1	Forced Expiratory Volume in 1 Second
FITC	Fluorescein Isothiocyanate
FVC	Forced Vital Capacity
HeLa	Cervical cancer Henrietta Lacks cell line
HepG2	Hepatoma G2 cell line
IS	Intermediate D-sorbitol solution
MDCK	Madin-Darby Canine Kidney
MLC	Myosin light chain
MIN6m9	Mouse pancreatic beta cell line
MOI	Multiplicity of infection
OWB	Organoid washing buffer
PerCP	Phycoerythrin Peridinin Chlorophyll Protein Complex
PI	Propidium iodure
ROCK	Rho-associated protein kinase
RV16	Rhinovirus 16

Introduction

Chronic obstructive diseases such as chronic obstructive pulmonary disease (COPD) and asthma are major public health challenges characterized by airflow limitation. Specific curative treatments are still lacking in these diseases at least because of the paucity of integrative approaches to decipher their pathophysiology, specially that of the distal airways. On the one hand, animal and especially rodent models are widely used for pre-clinical studies, but their airways differ anatomically, histologically and physiologically from those of humans, and they do not fully recapitulate disease hallmarks [1]. So far, they predict poorly which drugs will help treating patients with chronic obstructive diseases. On the other hand, the lung has a complex structure leading to a peculiar stiffness and 3D conformation that is hardly modeled *in vitro*, underlying the need to create adequate complex cellular models.

Various strategies have been proposed to model *in vitro* the conducting human bronchi [2]. 2D culture of bronchial epithelial cells at the air-liquid interface (ALI) allows the reconstitution of a fully differentiated epithelium with a functional ciliated function, with an easy access to apical and basal sides [3, 4], but it does not reproduce the three-dimensional architecture essential to model properly the airways. 3D bioprinting is a promising method to build tissue with a relevant geometry [5, 6], especially with the recent development of suitable bioinks, such as those composed of alginate and decellularized tissue, enabling the printing of a tubular structure [7]. However, the length of the tubes obtained is limited, and 3D printing of the last branches of the bronchial tree remains below the resolution limit of current bioprinting techniques. Elegant microfluidic approach has been used to design the so-called « airway-on-a-chip » [8, 9], providing unique advantages such as the ability to perfuse air, particles or nebulize drugs, to incorporate immune cells and the potential application of cyclic stretch to reproduce breathing movements. If the micro-engineered scaffold restrict

morphogenesis to predefined geometry, it does not completely match the exact topology of a bronchi, and does not offer a permissive and remodelable environment.

Others, starting from Benali *et al*.[10] to more recent ones [11–13] have favoured the 3rd dimension with « bronchospheres », in which bronchial epithelial cells, are embedded in a gel and self-organize into spheres with a liquid-filled lumen [14]. These self-renewing organoids exhibite ciliary activity and mucus production. In most of the bronchospheres, the apical side of the cells is facing the inside of the organoid, limiting the access to the lumen, although protocols to reverse airway organoid polarity have been developed [15, 16]. This closed and spherical architecture also impairs the removal of the dead cells inside, and the introduction of an air-liquid interface. Last, formation of invasive tubular from lung organoids have been observed [17], but it remains a stochastic and rather limited process.

The Cellular Capsule Technology, adapted from a co-extrusion microfluidic technique, has been used to encapsulate cells and extracellular matrix proteins in a tubular scaffold made of alginate gel [18]. Cell-laden microfibres have been generated with various cell types, such as endothelial cells, epithelial cells, fibroblasts, skeletal muscle cells and nerve cells [18]. When co-encapsulated, endothelial and vascular smooth muscle cells self-organized into tubular structures modeling vessels [19]. If epithelial cell lines such as the human hepatoma G2 (HepG2) cell line, the mouse pancreatic beta cell (MIN6m9) cell line, the cervical cancer Henrietta Lacks (HeLa) cell line, the Madin-Darby Canine Kidney (MDCK) cell line and the EpH4-J3B1A mammary gland epithelial cell line, have been previously successfully entubulated [18, 20], the behaviour of primary bronchial epithelial cells in this culture system has never been implemented.

Here, we aimed at building a tubular organoid-like model of distal airways, built with human primary bronchial epithelial cells. By providing a tubular template made of alginate using the Cellular Capsule Technology, we were able to drive the spontaneous self-organisation of lung

epithelial cells to obtain a 3D “bronchioid” model, with physiologically relevant shape and size. Importantly, the tubular geometry allows lumen access to create an air-liquid interface.

Methods

Patients

Macroscopically normal lung resection material for the purification of basal epithelial cells was obtained from a cohort of patients requiring thoracic lobectomy surgery for nodule or cancer (pN0) (*i.e.*, TUBE, sponsored by the University hospital of Bordeaux, which includes its own local ethic committee (CHUBX 2020/54)). According to the French law and the MR004 regulation, patients received an information form, allowing them to refuse the use of their surgical samples for research. The research was conducted according to the principles of the World Medical Association Declaration of Helsinki. A total of 10 COPD patients with a clinical diagnosis of COPD according to the GOLD guidelines [21] and 18 non-COPD subjects with normal lung function testing (*i.e.*, $FEV_1/FVC > 0.70$) were recruited from the University Hospital of Bordeaux (Table 1). A total of 5 other patients was also recruited from the TUBE cohort for the comparison of bronchioids to classical ALI cultures (Table E1). All clinical data were collected in the Clinical Investigation Center (CIC1401) from the University Hospital of Bordeaux.

Bronchial epithelial cell culture

Human basal bronchial epithelial cells (BECs) were derived from bronchial specimens as described previously [22]. Bronchial epithelial tissue was cultured in PneumaCult™-Ex medium (Stemcell Technologies, Vancouver, Canada) under water-saturated 5% CO_2 atmosphere at 37°C until basal BECs reached 80-90% confluence. For ALI culture, basal BEC were plated (1.10^5 cells per well) on tissue culture treated nucleopore membranes (Ref 3470, 6.5-mm diameter, 0.4-µm pore size, Transwell, Costar) in PneumaCult™-ALI Medium (Stemcell Technologies) applied at the basal side only to establish the ALI. Cells were maintained in culture for 9 or 21 days.

Microfluidic co-extrusion device and bronchioid formation

The design of a co-extrusion microfluidic device dedicated for bronchioid formation has been previously described for vessels [19]. Using this device with a 450 µm-diameter nozzle, we produced alginate hollow tubes filled with basal BECs. Cells were harvested by using 0.05% trypsin-EDTA (Ethylene Diamine Tetra-acetic Acid, Fisher Scientific) and resuspended in Matrigel (Corning, New York, USA) and Dulbecco's Modified Eagle Medium (Sigma-Aldrich, Saint Quentin-Fallavier, France), both varied from 33.5 to 35% (v/v). Cell loading of the core cell suspension (CCS) varied from 30 to 33% (v/v). Cells were then injected into the central zone isolated from a 2.5% (w/v) alginate solution (AS) (Protanal LF 200 S, FMC corporation, Philadelphia, United States) by a 300 mM intermediate D-sorbitol solution (IS) (Sigma-Aldrich). The experiments were performed using the following injection flow rates: 2 mL/hour (AS), 1 mL/hour (IS), and 1 mL/hour (CCS). With these flow rates, the thickness of alginate walls is approximately 50 µm, resulting in a 350 µm diameter cell tube (Figure 1A). A 100 mM calcium bath at 37°C was used to trigger rapid gelation of the alginate gel while avoiding osmotic shock. Immediately after formation (within less than 10 min), the cell-laden tubes were transferred in Pneumacult™ Airway Organoid Seeding Medium (Stemcell Technologies) at 37°C. After 24 hours, the bronchioids were transferred in Pneumacult™ Airway Organoid Differentiation Medium (Stemcell Technologies) to initiate the differentiation. To inhibit the Rho-associated protein kinase (ROCK), the Airway Organoid Medium was supplemented with Y-27632 (Sigma-Aldrich) at a concentration of 10 µM. Mediums were changed daily.

Western blot

The bronchioids were assayed for myosin light chain (MLC) II and double-phospho-MLC (Thr18, Ser19; PP-MLC) levels by Western blotting. Total protein extracts were obtained by

transferring the bronchioids in Dulbecco's Phosphate Buffered Saline (DPBS, Sigma-Aldrich) for 30 minutes at 37°C with gentle agitation to dissolve alginate. After centrifugation, the pellet was suspended in RIPA Lysis Buffer (Santa Cruz Biotechnology, Dallas, Texas, USA) supplemented with protease inhibitor cocktail and calyculin A (Sigma-Aldrich). These extracts were loaded onto a 4-20 % SDS-PAGE gel (Bio-Rad, Hercules, California, USA), transferred onto nitrocellulose membrane and revealed with a rabbit anti-target antibody (see Table E2). HRP-coupled anti-rabbit secondary antibody was used for revelation using ChemiDoc imaging instrument (Bio-Rad). Protein expressions were normalized using total loading protein (Stain-free system, Bio-Rad).

Quantitative Real-Time PCR

Total RNAs were extracted from bronchioids using RNAeasy kit, according to the manufacturer's instructions (Qiagen, Hilden, Germany). Five hundred nanograms of RNA were reverse-transcribed using the iScript™ Reverse Transcription Supermix (BioRad). cDNA samples were then analysed by qPCR using Perfecta® SYBR® Green SuperMix (Quantabio) through the CFX Connect real-time PCR detection system (Bio-Rad). Primers (*PPIA*, Forward 5′-CGGGTCCTGGCATCTTGT-3′ and Reverse 5′-CAGTCTTGGCAGTGCAGATGA-3′; *RPL13*, Forward 5′-GGGAGCAAGGAAAGGGTCTTA-3′ and Reverse 5′-CACCTGGACAATTCTCCGAGT-3′; *GusB*, Forward 5′-CCATCTGGGTCTGGATCAAAA-3′ and Reverse 5′-TGAAATCGGCAAAATTCCAAAT-3′; *KRT5*, Forward 5′-GCATCACCGTTCCTGGGTAA-3′ and Reverse 5′-GACACACTTGACTGGCGAGA-3′; *TP63*, Forward 5′- CCTCAGGGAGCTGTTATCCG-3′, Reverse 5′-ATACTGGGCATGGCTGTTCC -3′; *SCGB1A1*, Forward 5′-TCCTCCACCATGAAACTCGC-3′ and Reverse 5′- AGGAGGGTTTCGATGACACG-3′;

DNAH5, Forward 5′- AGAGGCCATTCGCAAACGTA-3′ and Reverse 5′-CCCGGAAAATGGGCAAACTG-3′; *AGR2*, Forward 5′-AAGGCAGGTGGGTGAGGAAATC-3′ and Reverse 5′-GTCGAGAGTCCTTTGTGTCCTT-3′; *MUC5AC*, Forward 5′-TACTCCACAGACTGCACCAACTG-3′ and Reverse 5′- CGTGTATTGCTTCCCGTCAA-3′; *EPCAM*, Forward 5′-CCATGTGCTGGTGTGTGAAC-3′ and Reverse 5′-AACGCGTTGTGATCTCCTTCT-3′; *CDH1* Forward 5′-TTACTGCCCCCAGAGGATGA-3′ and Reverse 5′- TGCAACGTCGTTACGAGTCA-3′;) were purchased from Sigma-Aldrich. mRNA expression was determined using the comparative 2-ΔΔCt method and normalized to the mRNA expression level of endogenous reference (*PPIA*, *RPL13* and *GusB*).

Production of rhinovirus 16 (RV16)-GFP

The cDNA pA16-GFP plasmid encoding RV16-GFP, which contains the rhinovirus sequence downstream a T7 promoter, is a kind gift from Yury A Bochkov [23]. The reverse genetics technique developed by Lee et al [24] was used to produce functional RV16-GFP virions. Briefly, for the initial production, the pA16-GFP plasmid was linearized by incubation with the restriction enzyme EcI136II (EcoICRI, Thermo Scientific) at 10 U/µL. After purification using the QIAprep Spin MINI Prep Kit (Qiagen), the DNA was transcribed *in vitro* into RNA by T7 polymerase and then transfected into HeLa cells using lipofectamine (Invitrogen). Twenty-four hours after transfection, the virus produced was purified and titrated by digital PCR after extraction and retrotranscription (Transcriptomic Platform, university of Bordeaux).

Infection with RV16- GFP

An approximately 5 cm-long bronchioid at day 4 to 5 was tranfered into a DMEM-contraining petri dish of 32 mm diameter. The bronchioid was cannulated by a 30G needle (MicrolanceTM, Becton Dickinson, Franklin Lakes, USA) with a diameter of 300 µm, which is the order of magnitude of the inner diameter of bronchioid. The needle was then connected to a 200 µL-syringe, containing DMEM (Fisher Scientific, Illkirch, France) with RV16-GFP at a concentration of 10 000 particles/µL and supplemented with eosin at 0.1% (Clinisciences, Nanterre, France). The solution was manually injected into the bronchioid lumen, with a visual control thanks to the eosin solution. At 48h post-infection, supernatants were collected and frozen at -80°C for cytokine concentration measurements. The bronchioid was dissociated and the cells manually counted before being processed for FACS analysis. The volume of injection corresponds to the volume of the lumen, which was estimated between 1 µL and 3 µL, for 5 cm length-bronchioid containing between 12 000 and 40 000 cells, with measured lumen diameters between 200 µm. This allows to calculate a multiplicity of infection (MOI) between 0.5 and 1.5.

Cytokine production

Bronchioid medium was assayed 48h post-infection for IFN-β, IFN-λ1/3 and CXCL8 concentration by ELISA following the manufacturer's recommendations (BioTechne). Values below the detection limit were counted as zero.

Flow cytometry

For ALI culture, epithelial cells in ALI culture were washed in PBS containing 0.5% bovine serum albumin (BSA, Sigma-Aldrich) and 2 mM EDTA (Invitrogen, Fisher Scientific, Illkirch, France) during 4 min at 37°C, and harvested by incubating with 0.5% trypsin- 0.2% EDTA solution (Sigma-Aldrich) during 5 min, with the addition of of Trypsin Neutralizing

Solution to neutralize Trypsin (Lonza, Bâle, Suisse), as described in [25]. For bronchioids, alginate dissolution was obtained by incubating the epithelial cell-laden tubes in DPBS during 20 min under gentle agitation. Cells were then mechanically and enzymatically dissociated by pipetting and by incubating the suspension with 0.5% trypsin- 0.2% EDTA during 5 min. After centrifugation, the cell suspension was filtered through a 70-µm cell strainer (Corning) and immediately subjected to flow cytometry to test for rhinovirus infection. Alternatively, annexin V- Propidium iodide (Fisher Scientific) or DAPI (5µg/ml, Sigma-Aldrich) was used for the detection of apoptotic and dead cells, respectively, according to the manufacturer's instructions. For differentiation characterization, cells were stained with anti-EpCAM-Peridinin Chlorophyll Protein Complex (PerCP)-Cy5.5 or its isotype control (see Table E2), and then fixed, permeabilized using the Foxp3 buffer set (Fisher Scientific) or the IntraPrep Permeabilization Reagent Kit (Beckman Coulter). The cell pellet was then stained with anti-pan cytokeratin-FITC, anti-cytokeratin 5-Alexa Fluor 488, anti-acetylated-tubulin-PE, anti-MUC5AC-Alex Fluor 647 or their respective isotype control (see Table E2). FACS data were acquired using a Canto II 4-Blue 2-Violet 2-Red laser configuration (BD Biosciences). Flow cytometry analysis were performed using Diva 8 (BD Biosciences).

Immunostaining

Bronchioids were fixed by using 4% paraformaldehyde (Sigma-Aldrich) diluted in DPBS supplemented with calcium (Sigma-Aldrich) during 30 min at room temperature, and immunostained as described in [26]. Briefly, after fixation, permeabilization and blocking steps were successively performed by incubating the bronchioids with cold DPBS supplemented with calcium containing 0.1% (vol/vol) Tween (P1379, Sigma-Aldrich), and with cold organoid washing buffer (OWB) composed of PBS containing 2g/L of BSA and 0.1% (vol/vol) of Triton X-100 (Biosolve, Dieuze, France), at 4°C during 15 min. The

bronchioids were then incubated with primary antibodies diluated in OWB at 4°C overnight, with mild rocking (see Table E2). The bronchioids were washed three times with OWB during two hours each time, and then stained with secondary antibodies, DAPI and phalloidin diluted in OWB at 4°C overnight, with mild rocking (see Table E2), before three supplementary washes with OWB during two hours each time. Next, the bronchioids were transferred into a µ-slide 4 well chamber slide (Ibidi, Gräfelfing, Germany) and resuspended in a fructose–glycerol clearing solution composed of 60% (vol/vol) glycerol and 2.5 M fructose in dH_2O, or in DPBS supplemented with calcium.

Imaging

Fixed bronchioids were imaged using a confocal Leica SP8 WLL2 microscope on an inverted DMI6000 stand (Leica Microsystems, Mannheim, Germany), using a 20X multi-immersion (NA 0.75 HC Plan Apo CS2) objective. The white light laser 2 (WLL2) was used for excitation of Alexa Fluor 647, 568 and 488 by a range of 650 to 750 nm, 590 to 640 nm and 500 to 550 nm, respectively. The confocal microscope was also equipped with a diode laser at 405 nm. A range of 410-480 nm was used to excite DAPI. The scanning was done using a conventional scanner (400Hz). The image size was 1024x1024 pixels, with a pixel size of 0.568 µm and a voxel depth of 1.040 µm. Detection was achieved with 2 internal photomultiplier tubes (PMT) and 2 internal hybrid detectors. Fluorescence images were acquired with the LAS X software (Leica). Using the Fiji software, the background value was subtracted from the original image and the image contrast in the background-corrected image was adjusted. The images were then processed with the Imaris software (Oxford Instruments, version 9) for segmentation and 3D visualization. The “Clipping Plane” function was used to truncate the image along a given plane in 3D space.

Live imaging to analyse ciliary beating frequency was performed on an inverted Leica DMi8 microscope (Leica Microsystems, Wetzlar, Germany) equipped with a Flash 4.0 sCMOS camera (Hamamatsu, Hamamatsu, Japan). The illumination system used was a Cool LED PE-4000 (CoolLED, Andover, USA). The objective used was a HCX PL Fluotar L 40X dry 0.6 NA PH2. The 37°C/5%CO_2 atmosphere was created with an incubator box and a gaz heating system (Pecon GmbH, Erbach, Germany). Brightfield images were acquired with the MetaMorph software (Molecular Devices, Sunnyvale, USA) for 2 seconds at a frame rate of 1000 images/second, in 9-10 different fields of the bronchioid. The image size was 512 x 32 pixels, with a pixel size of 0.1625 µm. If needed, recursive alignment of the stack of images is performed using the plugin "StackReg" of the Fiji software. Regions of interest were selected on the image generated by a maximum intensity projection using the plugin "Stardist 2D" of the Fiji software. The mean gray intensity was measured in each of these regions over time. Fast Fourier Transformation analysis was applied using Microsoft Excel to retrieve the main frequency (ciliary beat frequency, CBF). In each area, the median CBF is determined from the CBF values in the regions of interest. 9-10 fields are evaluated per donor.

Perfusion

A 3-4 cm-long bronchioid was cannulated by a 30G needle (MicrolanceTM, Becton Dickinson, Franklin Lakes, USA) with a diameter of 300 µm. The needle was then connected to a microfluidic system (Fluigent, Le Kremlin-Bicêtre, France) composed of a microfluidic low-pressure generator (FLPG Plus), a microfluidic vacuum pressure-based controller (LineUp™ Push-PullTM), a Non-Invasive Flow Sensor (NIFS) for liquid or air perfusion and a reservoir with a pressurization cap (P-CAP). Air was injected into the lumen at one opened end of the bronchioid, at a continuous flow rate of 0.2 mL/min. Air was released in the medium from the opposite tube end, generating visible air bubbles. Imaging was performed

using an Olympus CKX53 microscope with an Olympus DP23 camera with objectives 10X or 20X. Perfusion by air was continued for 4 hours. After stopping the infusion, calcein (Invitrogen) is added to the culture medium at a final concentration of 1 μM and incubated for 15 min at 37°C.

scRNA-seq data acquisition and analysis

Single cell suspension was obtained from bronchioids at day 21 as described for flow cytometry analysis. Cell number and viability were determined by a Trypan Blue exclusion assay before proceeding with the 10X Genomics (Pleasanton, CA) protocol for 3' Transcript Capture and Single Cell Library Prep. Approximately 18000 cells were loaded on a 10X Chromium Next GEM Chip G. GEM generation, RT, cleanup, cDNA amplification, fragmenting, end repair & A-tail prep, and sample index tagging were performed using the Chromium Next GEM Single Cell 3' GEM, Library & Gel Bead Kit v3.1 per manufacturer's instructions.

Quantification of the libraries was performed using QubitTM 2.0 Fluorometer (ThermoFischer) and quality was checked by 2100 Bioanalyzer with High Sensitivity DNA kit (Agilent). Libraries were sequenced using a P3 flow cell on a NextSeq2000 in 100bp paired-end mode (Illumina) to a read depth of 111,543 mean reads/cell (patient1) and 103,719 mean reads/cell (patient2).

Raw sequencing data was aligned to the GRCh38 human genome assembly (Ensembl98) and transcripts were quantified using the Cellranger software suite (v7.1.0). Subsequently, count matrices were loaded into R (v4.2.3), and downstream analyses were conducted using the Seurat R package (v5.0.1, [27]). Cells were filtered based on mitochondrial gene counts (<10%) and number of detected genes per cell (>2000). Gene counts were log-normalized (NormalizeData, default parameters), and highly variable features (HVGs) were selected

(FindVariableFeatures, default parameters). Batch correction was applied utilizing the Seurat reciprocal principal component analysis (RPCA) workflow with "Patient" as covariate. A nearest neighbor graph was constructed (FindNeighbors, dims = 1:10), and a two dimensional embedding was computed with the Uniform Manifold Approximation and Projection (UMAP) algorithm (RunUMAP, dims = 1:10). Unsupervised clustering was performed using the Louvain algorithm (FindClusters, resolution = 0.5). Cell types were annotated based on the expression of known marker genes. Ionocytes and Hillock-like cells did not cluster separately in the unsupervised clustering due to their small cell number and were selected based on UMAP coordinates, as they exhibited clearly distinct locations on the UMAP representation. Differential gene expression analysis (DGE) was performed using the Wilcoxon rank-sum test implementation of the Seurat package (FindAllMarkers, only.pos = TRUE, min.pct = 0.25) and results of DGE can be found in Table E3. Additionally, cell types were predicted with the CellTypist [28] Python package (v2.1.0) using the Human_Lung_atlas.pkl as model, with majority voting enabled. CellTypist-predicted annotations were grouped into broader categories (e.g. 'Basal resting' and 'Suprabasal' were categorized as 'Basal') to facilitate comparability with the manual annotations. The Adjusted Rand Index (ARI) was computed to assess concordance between manual annotations and CellTypist predictions.

Primary lung tissue reference construction

Primary lung tissue scRNA-seq data along with associated cell type annotations, clinical metadata, and technical metadata were obtained from the full Human Lung Cell Atlas (HLCA) as disclosed in March 2024 (https://cellxgene.cziscience.com/collections/6f6d381a-7701-4781-935c-db10d30de293). Cells annotated as airway epithelium were extracted from the dataset. To ensure technical coherence of the primary tissue reference with bronchioid

data produced in the present study, only cells analyzed with 10X genomics 3' v2 or v3 assays and derived from fresh tissue were retained for reference construction. Gene counts were log-normalized and 3000 HVGs were selected and scaled for subsequent data integration using the Seurat RPCA workflow with "dataset" as covariate. A nearest neighbor graph was constructed, and a two-dimensional UMAP embedding was computed based on 30 RPCA dimensions.

Neighborhood correlation analysis

Neighborhood graph correlation-based similarity analysis [29] was employed to compare cell states in the bronchioid model to primary lung tissue from distinct anatomical locations based on the common coordinate framework (CCF) established in the HLCA [30]. Cells from the primary lung tissue reference (constructed as described above) were categorized into four CCF categories: CCF 0, corresponding to the inferior turbinate, CCF 0.36-0.5, corresponding to the trachea and the main bronchi, CCF 0.72-0.81, corresponding to lobular bronchi and distal lobular airways, and CCF 0.97, corresponding to the parenchyma [30]. For the bronchioid data as well as the primary lung tissue reference CCF categories, independent neighborhood graphs based on transcriptional similarity were constructed with the miloR package (v1.6.0) using k = 30 nearest neighbors and 30 RPCA dimensions of the respective data source [31]. The R package scrabbitr (v0.1.0) was used to calculate the mean expression profiles within each neighborhood and to compute the Pearson correlations of expression of the 3000 HVGs from the primary lung tissue reference, excluding mitochondrial genes, between all pairs of bronchioid and CCF category neighborhoods. The maximum correlation between each bronchioid neighborhood and a neighborhood in the CCF-stratified primary tissue reference was considered as measure of similarity.

Data and code availability

Single-cell RNA-sequencing data generated in the current study is available on Zenodo under 10.5281/zenodo.10834205. R code used for scRNA-seq data analysis has been deposited on GitHub: https://github.com/saliba-lab/Bronchioid_scRNAseq

Results

Basal bronchial epithelial cell cultures were obtained from 28 patients (Table 1, n= 18 non-COPD, n=10 COPD). Using the Cellular Capsule Technology, we encapsulated these bronchial epithelial cells in the presence of Matrigel, into tubular structures made of alginate (figure 1a). Of note, cells are injected at a concentration sufficient to allow immediate coverage of the entire alginate walls as soon as the tube is generated. Of the 28 samples, only one culture from non-COPD patient (4%) failed to generate bronchioid, due to a technical problem (figure E1). Nine bronchioids (n=4 non-COPD, n=5 COPD) were fully used before 9 days for early characterization (figure E1). Over the 18 bronchioids kept at least 11 days in culture, 5 (28%) are from patients with COPD, which is a proportion close to the composition of the recruited patient population. Altogether, it shows that bronchioids are generated with a high success rate, and that they can be kept in culture during several weeks, in a similar way for those derived from COPD and non-COPD patients.

Within the first 24h, epithelial cells formed a monolayer that indeed entirely covered the inner part of the tube (figure 1b). However, as previously shown with epithelial cell lines [20], the bronchioid collapsed 1-2 days after encapsulation (figure 1b). Inhibition of actomyosin contractibility using the Rho-associated protein kinase (ROCK) inhibitor Y-27632 (10 µM) prevented epithelial detachment (figure 1b), while decreasing the level of double-phospho-myosin light chain (Thr18, Ser19; PP-MLC) (figure 1c), suggesting that cell contractility was the main driving force for shrinkage.

Dissolution of the alginate gel was successfully obtained by calcium and magnesium cations depletion during 30 minutes, allowing the obtention of a cell suspension. Analysis of this suspension by flow cytometry demonstrated that the tubular structures remained stable and viable during at least 9 days (Figure 1d). Thus, in the next experiments, the bronchioids were continuously treated with Y-27632 to avoid the collapse. We confirmed the epithelial nature of cells by flow cytometry, showing that at day 1 the cells were almost all positive for

EpCAM and cytokeratin, as obtained with differentiated bronchial epithelial cells at the ALI (Table E1, figure 2a).

The mRNA level measured by RT-qPCR of *CDH1* (encoding E-cadherin) and *EPCAM* remained stable over time (figure 2b). Confocal imaging and 3D reconstruction demonstrated the organisation of bronchial cells into a tubular structure with a typical epithelial morphology and a visible lumen, reminiscent of the structure of distal bronchi (figure 2c). The presence of ZO-1 and actin fibers at cell-cell contacts attested the existence of tight junctions (figure 2d).

RT-qPCR revealed also that the expression of airway basal cell gene keratin 5 (*KRT5)* stayed stable, those of *TP63* progressively declined over time, whereas the club cell secretory marker secretoglobin family 1A member 1 (*SCGB1A1*) was highly upregulated (figure 3a). The expression of ciliated cell markers *FOXJ1* and *DNAH5*, those of the transcription factor anterior gradient 2 (*AGR2*) and the goblet cell marker mucin 5AC (*MUC5AC*) progressively increased in culture (figure 3a). At day 9, the expression of those genes was comparable with bronchial epithelial cells at the ALI for the same time, with the exception of *EPCAM*, *SCGB1A1*, *MUC5AC* whose levels are higher, and *AGR2* whose level is reduced in the ALI condition (figure 2b and 3a). The cellular composition and viability were very similar in three different portions sampled along the tube (figure E2), indicating a homogenous cellular structure throughout the bronchioid. By confocal microscopy, we found at day 11 ciliated cells located at the internal layer lining the bronchioid lumen (figure 3b, movie E1). Most goblet cells were also facing the lumen, with some MUC5AC-positive cells more externally localised (figure 3b). Positive staining for MUC5AC was also found inside the lumen, suggesting mucus secretion. Although all intermediate states of differentiation are probably not detected by simple stainings, especially during the last 2 weeks in culture, flow cytometry experiments confirmed the progressive loss of basal cells over time, with a concomitant increase of club, goblet and ciliated cells until day 21 (figure 3c-d).

To further characterize the bronchioid model, single-cell RNA-sequencing was conducted on bronchioids from two non-COPD patients after 21 days of culture (Methods). In total, 5,087 high-quality single cells (patient1 = 2,860 cells, patient2 = 2,227 cells) were analyzed (see Methods and figure E3a), which were categorized into 9 distinct populations without noticeable differences between the donors (figures 4a and E3b). These populations could be annotated based on established markers as basal (*KRT5*, *TP63*), secretory (*SCGB1A1*, *SCGB3A1*, *MUC5B*), goblet (*MUC5AC*, *CEACAM5*), deuterosomal (*FOXN4*, *CDC20B*), ciliated (*FOXJ1*, *TPPP3*), ionocyte (*FOXI1*, *CFTR*), and hillock-like (*KRT13*, *KRT14*) cells (figure 4a-b, Table E3). Additionally, populations of differentiating basal cells (*KRT5*, *AGR2*) and proliferating cells (*MKI67*) were identified. To validate manual cell type annotations, CellTypist [28] with the Human Lung Cell Atlas (HLCA) [30] model was employed for cell type prediction, demonstrating a high level of agreement (adjusted rand index = 0.691, figure E3c). Notably, all cell types, except for hillock-like cells (14 cells, 0.24 %), were consistently observed in bronchioids derived from both patients, although the proportions were not strictly identical (figures 4c and E3b). While differentiated secretory and multiciliated lineage cells, as well as rare ionocytes and Hillock-like cells, were revealed in our bronchioid scRNA-seq data, a distinct population of *SCGB3A2*+*SFTPB*+ terminal airway-enriched secretory cells (TASCs) [32, 33] was not identified as a cluster, despite the co-expression of marker genes in few cells (figure E3d-e). Finally, to evaluate whether the bronchioid model accurately recapitulates small airways specifically at the transcriptional level, data from the HLCA and the common coordinate framework (CCF) introduced therein were utilized [30]. A primary tissue reference across four distinct anatomical regions based on CCF was assembled, comprising cells from eight datasets marked broadly as airway epithelium in the HLCA (see Methods, figure E4a-c). Bronchioid model cell states were compared to this primary tissue reference by performing a neighborhood graph correlation-based similarity analysis ([29], see

Methods). Overall, greater similarity to cell states from the airways (CCF 0.32-0.5 and CCF 0.72-0.81) was exhibited by bronchioid cell states than to those from the nose (CCF 0) or parenchyma (CCF 0.97). Comparing upper and lower airways, the similarity analysis results indicated that cell states from the distal airways (CCF 0.72-0.81) tended to be more closely resembled by bronchioid cell states (figure 4d-e). In summary, these data are consistent with the induction of distal airway fate in bronchioids, with identified cell states recapitulating distal airway epithelial cells at a global transcriptional level with high fidelity, and differentiated cells localized to their corresponding *in vivo* positions.

Using high-speed video microscopy [34], ciliary beating was observed in the bronchioid model (movie E2). For bronchioids generated from 4 different patients, we determined the median ciliary beat frequency (CBF) across different fields of acquisition (figure 5a-b). Overall, median CBF values ranges ranged from 6Hz to 27Hz (figure 5c), which is in the range of *in vivo* reference CBF [35], and that are also very comparable to those found in bronchial epithelial strips [36], ALI culture [37] and airway organoids [38]. Interestingly, CBF values significant decreased in the bronchoids derived from patients with COPD in comparison to non-COPD patients (figure 5c). This is fully in agreement with the reduced cilia beating frequency shown in nasal cilia samples [39, 40] and airway organoids [38] from COPD patients, demonstrating the potential of the bronchioid model to model respiratory diseases.

We also used the model to test rhinovirus infection, a major trigger of asthma and COPD exacerbation [41, 42]. To track viral infection, we injected into the lumen of the bronchioid a recombinant rhinovirus type 16 (RV16) accommodating green fluorescent protein (GFP) expression [23] (figure 6a). Considering the calculated volume of the injection, estimated between 1 µL and 3 µL for a 5 cm length-bronchioid containing between 12 000 and 40 000 cells, with measured lumen diameters between 200 µm, the multiplicity of infection (MOI)

was around 0.5 and 1.5. Forty-eight hours post-infection, 95% and 81% of the cells were GFP-positive in bronchioids generated from patients 3 and 4, respectively (figure 6b-c), suggesting infection and viral RNA replication in a vast majority of cells, in agreement with the calculated MOI. The infection was less efficient (45% of GFP-positive cells) in bronchioid generated from patient 5 (figure 6b-c). Next, we examined effects of RV16 on cytokine secretion, including the type I (IFN-β) β and type III (IFN-λ1/3) interferons and the chemokine CXCL8. RV16-GFP infection increased the level of secreted IFN-β, IFN- λ1/3 and CXCL8, in comparison with the non-infected bronchioid condition for patients 3 and 4 (figure 6d). No induction of interferon production and a modest increase of CXCL8 level were observed in bronchioid generated from patient 5, in agreement with a lower infection efficiency (figure 6d).

To introduce an air-liquid interface, a 30G needle was inserted at day 3 in the lumen of the bronchioid and connected to a dedicated perfusion system (figure 7a). We injected air, as shown by a change of refringence (figure 7a, movie E3), and we maintained perfusion for 4 hours, by adjusting the flow rate to match the circulating flow in distal bronchi with an internal diameter of 400 µm, *i.e.*, 0.2 mL/min. Calcein staining indicated that cells remained viable after 4h of air perfusion (figure 7b). Air exposure show a systematic up-regulation of *SCGB1A1* in all the bronchioids perfused during 4h (figure 7c). The expression of other genes tested shows either no variation (*TP63*, *KRT5*, *FOXJ1*, *AGR2*) or changes dependent on the experiments (*DNAH5*, *MUC5AC*). Although a longer time of perfusion may be required to observe more robust effects, this indicates the the potential of ALI to affect differentiation in the bronchioid model.

Discussion

Taken together, our bronchioid model offers several key advantages compared with current distal bronchial culture systems. In particular, in comparison with the classical 2D ALI model, the main advantages of our tubular system are the third dimension and the relevant geometry and stiffness, preventing the apparition of a non-physiologic population by epithelial-mesenchymal transition [43]. Compared with airway organoid, the bronchioid model also offers the tubular geometry, lumen access for air exposure and viral infection, while retaining major characteristics of the airway epithelium. This system is also compatible with multiple biological analyzes such as immunohistochemistry, flow cytometry, transcriptomics and immunoblotting. We expect this model to be instrumental in uncovering cellular mechanisms leading to airflow obstruction and for implementing efficient drug testing assays.

Inhibiting the ROCK pathway is considered important for lung organoid generation [44], because of its anti-apoptotic and proliferative effects [45]. We showed here that downregulation of the MLC activity through the ROCK inhibitor Y-27632 was also required to facilitate the generation of an epithelial tubular structure that did not collapse. Importantly, alteration of ROCK activity did not prevent cell-cell adhesion and epithelial differentiation, demonstrating the key role of 3D geometry and subtrate stiffness.

The incorporation of primary bronchial epithelial cells into 3D bioengineered structures is challenging, due in particular to the low attachement capacities of these cells to artificial substrates. The bronchioid collapse observed in the absence of ROCK inhibition may also result from insufficient adhesion to the inert alginate walls. Interestingly, tube collapse has also been observed during early lung development [46]. Thus, it is likely that there is further room for improvement of bronchioid development, by favouring epithelial cell adhesion to the scaffold [7, 47] or by modulating luminal pressure [46].

Together with the demonstration of progressive differentiation into ciliated and goblet cells, we provide evidence of ciliary function and mucus production, showing that the bronchioid model very likely displays the fundamental mucociliary clearance property. We also demonstrate that bronchioids derived from cells COPD patients recapitulate important pathological features of COPD, including an impaired ciliary beating function. At day 21, the cellular composition of the bronchioid is similar to those of airway organoids [11], with a percentage of goblet cells even slightly decreased compared to lung organoids. ScRNA sequencing analysis confirmed the identification of the major bronchial epithelial cell types in proportions intermediate between those of proximal and distal airways [33], together with a high level of similarity between the bronchioid and distal airway cell types on the transcriptional level. Thus, the dimension and the geometry of the bronchioid model, closed to a 17th generation bronchiole, as well as its general composition, make it a relevant model of distal airway. However, the cellular composition is not strictly similar to those of distal airways, with in particular the absence of *SCGB3A2+ SFTPB+* terminal airway-enriched secretory cells (TASCs), a cell population specific to distal airways [32, 33]. This is a limitation of the bronchioid model, which can be attributed to the proximal basal cells used in this study [32, 33], and/or to the absence of air exposure for this experiment. Indeed, our perfusion experiments indicated that the introduction of the air-liquid interface (ALI) during 4h induced an up-regulation of *SCGB1A1* level (figure 6c). Although this requires further studies, these effects are consistent with a shift toward a distal phenotype [48], and suggest that the potential of the bronchioid model at the ALI to fully model of distal airways.

While lung organoids have been used to study infection by viruses such as syncytial virus (RSV) [11], enterovirus [49], influenza [12, 50], and acute respiratory syndrome coronavirus 2 (SARS-CoV-2) [38, 51–53], the infection usually requires organoid re-orientation to achieve apical-out polarity [53, 54]. Polarity reversal by suspension culture requires

extracellular matrix (ECM) removal, losing the 3D-relevant environment and possibly affecting mechanostransduction pathways. In addition, this step takes at least 1-2 days and does not work at 100%. More importantly, this procedure affects cell viability in differentiated organoid, restricting its use for undifferentiated organoids. In the bronchioid model, we demonstrated efficient rhinoviral infection through intraluminal virus injection, as well as epithelial response. In contrast to microinjection into the center of spherical organoid [55] or organoid mechanical disruption to expose the apical surface [56], our method does not affect the organoid wall, by taking advantage of the easy access to the lumen in the bronchioid model. This procedure is compatible with many types of downstream analyses, including flow cytometry and biochemistry techniques. Of note, the concentration of IFN-λ1/3 in the medium appears lower that those measured in ALI culture following rhinovirus infection [57], which could be explained the fact that the volume of medium is much higher relatively to the number of cells in our settings. In total, our results demonstrate the value of bronchioid technology to study infectious diseases and host–pathogen interactions.

In conclusion, we have generated a new workflow that allows the efficient generation of tubular structures modeling distal airways, built with epithelial cells derived from clinical samples. These bronchioids are susceptible to be perfused with liquid, and more importantly with air to establish an ALI. As meters of tubes are generated per condition and the duration of the assay is relatively short, it also offers the opportunity to apply high throughput methods, in particular for drug screening and testing, in the context of respiratory disease modelling.

Acknowledgments

We thank the study participants and the staff of the Thoracic Surgery, Respiratory, Lung Function Testing departments from the University Hospital of Bordeaux (Bordeaux, France), Isabelle Goasdoue, Isabelle Bernis, Natacha Robert, Virginie Niel, and Marine Servat from the clinical investigation center for technical assistance, and Atika Zouine, Vincent Pitard and Xavier Gautherau for technical assistance at the Flow cytometry and OneCell facilities (CNRS UMS 3427, INSERM US 005, Univ. Bordeaux, F-33000 Bordeaux, France), Christel Poujol, Magali Mondin, Sébastien Marais and Fabrice Cordelières for help with imaging and image analysis et the Bordeaux Imaging Centre (BIC; Bordeaux, France). Microscopy was performed at BIC, a service unit of the CNRS-INSERM and Bordeaux University, a member of the national BioImaging infrastructure of France supported by the French National Research Agency (ANR-10-INBS-04). AES and AML thank the Deutsche Forschungsgemeinschaft DFG SFB 1583 (project number 492620490; Z2 project) and AES thanks the DFG GRK2157 for funding. AES, AML and TK thank the CoreUnitSysmed for technical support for sequencing.

Funding: The project was funded by :

the “Agence Nationale de la Recherche” (ANR-21-CE18-0001-01) (ID)

the “Region Nouvelle Aquitaine” (ID) (AAPR2022A- 2021-16982910 and AAPR2022I-2021-16983510)

the “Departement Sciences et Technologies” of the Bordeaux University (ID)

the “Institut Universitaire de France” (IUF) (ID)

References

1. Ghorani V, Boskabady MH, Khazdair MR, Kianmeher M. Experimental animal models for COPD: a methodological review. *Tob Induc Dis* 2017; 15: 25.
2. Nizamoglu M, Joglekar MM, Almeida CR, Larsson Callerfelt A-K, Dupin I, Guenat OT, Henrot P, van Os L, Otero J, Elowsson L, Farre R, Burgess JK. Innovative three-dimensional models for understanding mechanisms underlying lung diseases: powerful tools for translational research. *Eur Respir Rev* 2023; 32: 230042.
3. Jorissen M, Van der Schueren B, Van den Berghe H, Cassiman JJ. Contribution of in vitro culture methods for respiratory epithelial cells to the study of the physiology of the respiratory tract. *Eur Respir J* 1991; 4: 210–217.
4. Adler KB, Cheng PW, Kim KC. Characterization of guinea pig tracheal epithelial cells maintained in biphasic organotypic culture: cellular composition and biochemical analysis of released glycoconjugates. *Am J Respir Cell Mol Biol* 1990; 2: 145–154.
5. Dabaghi M, Carpio MB, Moran-Mirabal JM, Hirota JA. 3D (bio)printing of lungs: past, present, and future. *Eur Respir J* 2023; 61: 2200417.
6. De Santis MM, Bölükbas DA, Lindstedt S, Wagner DE. How to build a lung: latest advances and emerging themes in lung bioengineering. *Eur Respir J* 2018; 52.
7. De Santis MM, Alsafadi HN, Tas S, Bölükbas DA, Prithiviraj S, Da Silva IAN, Mittendorfer M, Ota C, Stegmayr J, Daoud F, Königshoff M, Swärd K, Wood JA, Tassieri M, Bourgine PE, Lindstedt S, Mohlin S, Wagner DE. Extracellular-Matrix-Reinforced Bioinks for 3D Bioprinting Human Tissue. *Adv Mater* 2021; 33: e2005476.
8. Huh D, Matthews BD, Mammoto A, Montoya-Zavala M, Hsin HY, Ingber DE. Reconstituting organ-level lung functions on a chip. *Science* 2010; 328: 1662–1668.
9. Benam KH, Villenave R, Lucchesi C, Varone A, Hubeau C, Lee H-H, Alves SE, Salmon M, Ferrante TC, Weaver JC, Bahinski A, Hamilton GA, Ingber DE. Small airway-on-a-chip enables analysis of human lung inflammation and drug responses in vitro. *Nat Methods* 2016; 13: 151–157.
10. Benali R, Tournier JM, Chevillard M, Zahm JM, Klossek JM, Hinnrasky J, Gaillard D, Maquart FX, Puchelle E. Tubule formation by human surface respiratory epithelial cells cultured in a three-dimensional collagen lattice. *Am J Physiol* 1993; 264: L183-192.
11. Sachs N, Papaspyropoulos A, Zomer-van Ommen DD, Heo I, Böttinger L, Klay D, Weeber F, Huelsz-Prince G, Iakobachvili N, Amatngalim GD, de Ligt J, van Hoeck A, Proost N, Viveen MC, Lyubimova A, Teeven L, Derakhshan S, Korving J, Begthel H, Dekkers JF, Kumawat K, Ramos E, van Oosterhout MF, Offerhaus GJ, Wiener DJ, Olimpio EP, Dijkstra KK, Smit EF, van der Linden M, Jaksani S, et al. Long-term expanding human airway organoids for disease modeling. *The EMBO Journal* John Wiley & Sons, Ltd; 2019; 38: e100300.
12. Zhou J, Li C, Sachs N, Chiu MC, Wong BH-Y, Chu H, Poon VK-M, Wang D, Zhao X, Wen L, Song W, Yuan S, Wong KK-Y, Chan JF-W, To KK-W, Chen H, Clevers H, Yuen K-Y. Differentiated human airway organoids to assess infectivity of emerging influenza virus. *Proc Natl Acad Sci U S A* 2018; 115: 6822–6827.
13. Lamers MM, van der Vaart J, Knoops K, Riesebosch S, Breugem TI, Mykytyn AZ, Beumer J, Schipper D, Bezstarosti K, Koopman CD, Groen N, Ravelli RBG, Duimel HQ, Demmers JAA, Verjans GMGM, Koopmans MPG, Muraro MJ, Peters PJ, Clevers H, Haagmans BL. An organoid-derived bronchioalveolar model for SARS-CoV-2 infection of human alveolar type II-like cells. *The EMBO Journal* John Wiley & Sons, Ltd; 2020; n/a: e105912.
14. Hiemstra PS, Tetley TD, Janes SM. Airway and alveolar epithelial cells in culture. *Eur Respir J* 2019; 54: 1900742.
15. Boecking CA, Walentek P, Zlock LT, Sun DI, Wolters PJ, Ishikawa H, Jin B-J, Haggie PM, Marshall WF, Verkman AS, Finkbeiner WE. A simple method to generate human airway epithelial organoids with externally orientated apical membranes. *Am J Physiol Lung Cell Mol Physiol* 2022; 322: L420–L437.
16. Stroulios G, Brown T, Moreni G, Kondro D, Dei A, Eaves A, Louis S, Hou J, Chang W, Pajkrt D, Wolthers KC, Sridhar A, Simmini S. Apical-out airway organoids as a platform for studying

viral infections and screening for antiviral drugs. *Sci Rep* Nature Publishing Group; 2022; 12: 7673.

17. Tan Q, Choi KM, Sicard D, Tschumperlin DJ. Human Airway Organoid Engineering as a Step toward Lung Regeneration and Disease Modeling. *Biomaterials* 2017; 113: 118–132.
18. Onoe H, Okitsu T, Itou A, Kato-Negishi M, Gojo R, Kiriya D, Sato K, Miura S, Iwanaga S, Kuribayashi-Shigetomi K, Matsunaga YT, Shimoyama Y, Takeuchi S. Metre-long cell-laden microfibres exhibit tissue morphologies and functions. *Nature Mater* Nature Publishing Group; 2013; 12: 584–590.
19. Andrique L, Recher G, Alessandri K, Pujol N, Feyeux M, Bon P, Cognet L, Nassoy P, Bikfalvi A. A model of guided cell self-organization for rapid and spontaneous formation of functional vessels. *Sci Adv* 2019; 5: eaau6562.
20. Maechler FA, Allier C, Roux A, Tomba C. Curvature-dependent constraints drive remodeling of epithelia. *J Cell Sci* 2019; 132: jcs222372.
21. Global Initiative for Chronic Obstructive Lung Disease [Internet]. Global Initiative for Chronic Obstructive Lung Disease - GOLD [cited 2023 Feb 6].Available from: https://goldcopd.org/.
22. Trian T, Allard B, Dupin I, Carvalho G, Ousova O, Maurat E, Bataille J, Thumerel M, Begueret H, Girodet P-O, Marthan R, Berger P. House dust mites induce proliferation of severe asthmatic smooth muscle cells via an epithelium-dependent pathway. *Am. J. Respir. Crit. Care Med.* 2015; 191: 538–546.
23. Olszewski D, Georgi F, Murer L, Andriasyan V, Kuttler F, Petkidis A, Witte R, Yakimovich A, Fischer L, Rozanova A, Yamauchi Y, Turcatti G, Greber UF. High-content, arrayed compound screens with rhinovirus, influenza A virus and herpes simplex virus infections. *Sci Data* Nature Publishing Group; 2022; 9: 610.
24. Lee W-M, Wang W, Bochkov YA, Lee I. Reverse genetics system for studying human rhinovirus infections. *Methods Mol Biol* 2015; 1221: 149–170.
25. Maestre-Batlle D, Pena OM, Hirota JA, Gunawan E, Rider CF, Sutherland D, Alexis NE, Carlsten C. Novel flow cytometry approach to identify bronchial epithelial cells from healthy human airways. *Sci Rep* Nature Publishing Group; 2017; 7: 42214.
26. Dekkers JF, Alieva M, Wellens LM, Ariese HCR, Jamieson PR, Vonk AM, Amatngalim GD, Hu H, Oost KC, Snippert HJG, Beekman JM, Wehrens EJ, Visvader JE, Clevers H, Rios AC. High-resolution 3D imaging of fixed and cleared organoids. *Nat Protoc* Nature Publishing Group; 2019; 14: 1756–1771.
27. Hao Y, Stuart T, Kowalski MH, Choudhary S, Hoffman P, Hartman A, Srivastava A, Molla G, Madad S, Fernandez-Granda C, Satija R. Dictionary learning for integrative, multimodal and scalable single-cell analysis. *Nat Biotechnol* Nature Publishing Group; 2024; 42: 293–304.
28. Domínguez Conde C, Xu C, Jarvis LB, Rainbow DB, Wells SB, Gomes T, Howlett SK, Suchanek O, Polanski K, King HW, Mamanova L, Huang N, Szabo PA, Richardson L, Bolt L, Fasouli ES, Mahbubani KT, Prete M, Tuck L, Richoz N, Tuong ZK, Campos L, Mousa HS, Needham EJ, Pritchard S, Li T, Elmentaite R, Park J, Rahmani E, Chen D, et al. Cross-tissue immune cell analysis reveals tissue-specific features in humans. *Science* American Association for the Advancement of Science; 2022; 376: eabl5197.
29. Ton M-LN, Keitley D, Theeuwes B, Guibentif C, Ahnfelt-Rønne J, Andreassen TK, Calero-Nieto FJ, Imaz-Rosshandler I, Pijuan-Sala B, Nichols J, Benito-Gutiérrez È, Marioni JC, Göttgens B. An atlas of rabbit development as a model for single-cell comparative genomics. *Nat Cell Biol* Nature Publishing Group; 2023; 25: 1061–1072.
30. Sikkema L, Ramírez-Suástegui C, Strobl DC, Gillett TE, Zappia L, Madissoon E, Markov NS, Zaragosi L-E, Ji Y, Ansari M, Arguel M-J, Apperloo L, Banchero M, Bécavin C, Berg M, Chichelnitskiy E, Chung M, Collin A, Gay ACA, Gote-Schniering J, Hooshiar Kashani B, Inecik K, Jain M, Kapellos TS, Kole TM, Leroy S, Mayr CH, Oliver AJ, von Papen M, Peter L, et al. An integrated cell atlas of the lung in health and disease. *Nat Med* Nature Publishing Group; 2023; 29: 1563–1577.
31. Dann E, Henderson NC, Teichmann SA, Morgan MD, Marioni JC. Differential abundance testing on single-cell data using k-nearest neighbor graphs. *Nat Biotechnol* Nature Publishing Group; 2022; 40: 245–253.

32. Kadur Lakshminarasimha Murthy P, Sontake V, Tata A, Kobayashi Y, Macadlo L, Okuda K, Conchola AS, Nakano S, Gregory S, Miller LA, Spence JR, Engelhardt JF, Boucher RC, Rock JR, Randell SH, Tata PR. Human distal lung maps and lineage hierarchies reveal a bipotent progenitor. *Nature* 2022; 604: 111–119.
33. Rustam S, Hu Y, Mahjour SB, Rendeiro AF, Ravichandran H, Urso A, D'Ovidio F, Martinez FJ, Altorki NK, Richmond B, Polosukhin V, Kropski JA, Blackwell TS, Randell SH, Elemento O, Shaykhiev R. A Unique Cellular Organization of Human Distal Airways and Its Disarray in Chronic Obstructive Pulmonary Disease. *Am J Respir Crit Care Med* 2023; 207: 1171–1182.
34. Jackson CL, Bottier M. Methods for the assessment of human airway ciliary function. *Eur Respir J* 2022; 60: 2102300.
35. Low PM, Luk CK, Dulfano MJ, Finch PJ. Ciliary beat frequency of human respiratory tract by different sampling techniques. *Am Rev Respir Dis* 1984; 130: 497–498.
36. Thomas B, Rutman A, Hirst RA, Haldar P, Wardlaw AJ, Bankart J, Brightling CE, O'Callaghan C. Ciliary dysfunction and ultrastructural abnormalities are features of severe asthma. *Journal of Allergy and Clinical Immunology* 2010; 126: 722-729.e2.
37. Hirst RA, Jackson CL, Coles JL, Williams G, Rutman A, Goggin PM, Adam EC, Page A, Evans HJ, Lackie PM, O'Callaghan C, Lucas JS. Culture of Primary Ciliary Dyskinesia Epithelial Cells at Air-Liquid Interface Can Alter Ciliary Phenotype but Remains a Robust and Informative Diagnostic Aid. *PLOS ONE* Public Library of Science; 2014; 9: e89675.
38. Chan LLY, Anderson DE, Cheng HS, Ivan FX, Chen S, Kang AEZ, Foo R, Gamage AM, Tiew PY, Koh MS, Lee KCH, Nichol K, Pathinayake PS, Chan YL, Yeo TW, Oliver BG, Wark PAB, Liu L, Tan NS, Wang L-F, Chotirmall SH. The establishment of COPD organoids to study host-pathogen interaction reveals enhanced viral fitness of SARS-CoV-2 in bronchi. *Nat Commun* Nature Publishing Group; 2022; 13: 7635.
39. Yaghi A, Zaman A, Cox G, Dolovich MB. Ciliary beating is depressed in nasal cilia from chronic obstructive pulmonary disease subjects. *Respiratory Medicine* Elsevier; 2012; 106: 1139–1147.
40. Piatti G, Ambrosetti U, Santus P, Allegra L. Effects of salmeterol on cilia and mucus in COPD and pneumonia patients. *Pharmacol Res* 2005; 51: 165–168.
41. Wedzicha JA. Role of Viruses in Exacerbations of Chronic Obstructive Pulmonary Disease. *Proc Am Thorac Soc* American Thoracic Society - PATS; 2004; 1: 115–120.
42. Message SD, Laza-Stanca V, Mallia P, Parker HL, Zhu J, Kebadze T, Contoli M, Sanderson G, Kon OM, Papi A, Jeffery PK, Stanciu LA, Johnston SL. Rhinovirus-induced lower respiratory illness is increased in asthma and related to virus load and Th1/2 cytokine and IL-10 production. *Proceedings of the National Academy of Sciences* Proceedings of the National Academy of Sciences; 2008; 105: 13562–13567.
43. Greaney AM, Adams TS, Brickman Raredon MS, Gubbins E, Schupp JC, Engler AJ, Ghaedi M, Yuan Y, Kaminski N, Niklason LE. Platform Effects on Regeneration by Pulmonary Basal Cells as Evaluated by Single-Cell RNA Sequencing. *Cell Rep* 2020; 30: 4250-4265.e6.
44. Kim J, Koo B-K, Knoblich JA. Human organoids: model systems for human biology and medicine. *Nat Rev Mol Cell Biol* 2020; 21: 571–584.
45. Watanabe K, Ueno M, Kamiya D, Nishiyama A, Matsumura M, Wataya T, Takahashi JB, Nishikawa S, Nishikawa S, Muguruma K, Sasai Y. A ROCK inhibitor permits survival of dissociated human embryonic stem cells. *Nat Biotechnol* Nature Publishing Group; 2007; 25: 681–686.
46. Conrad L, Runser SVM, Fernando Gómez H, Lang CM, Dumond MS, Sapala A, Schaumann L, Michos O, Vetter R, Iber D. The biomechanical basis of biased epithelial tube elongation in lung and kidney development. *Development* 2021; 148: dev194209.
47. Hamilton NJI, Lee DDH, Gowers KHC, Butler CR, Maughan EF, Jevans B, Orr JC, McCann CJ, Burns AJ, MacNeil S, Birchall MA, O'Callaghan C, Hynds RE, Janes SM. Bioengineered airway epithelial grafts with mucociliary function based on collagen IV- and laminin-containing extracellular matrix scaffolds. *Eur Respir J* 2020; 55: 1901200.
48. Yang J, Zuo W-L, Fukui T, Chao I, Gomi K, Lee B, Staudt MR, Kaner RJ, Strulovici-Barel Y, Salit J, Crystal RG, Shaykhiev R. Smoking-Dependent Distal-to-Proximal Repatterning of the Adult Human Small Airway Epithelium. *Am J Respir Crit Care Med* 2017; 196: 340–352.

49. van der Sanden SMG, Sachs N, Koekkoek SM, Koen G, Pajkrt D, Clevers H, Wolthers KC. Enterovirus 71 infection of human airway organoids reveals VP1-145 as a viral infectivity determinant. *Emerging Microbes & Infections* Taylor & Francis; 2018; 7: 1–9.
50. Hui KPY, Ching RHH, Chan SKH, Nicholls JM, Sachs N, Clevers H, Peiris JSM, Chan MCW. Tropism, replication competence, and innate immune responses of influenza virus: an analysis of human airway organoids and ex-vivo bronchus cultures. *The Lancet. Respiratory Medicine* 2018; 6: 846–854.
51. Han Y, Duan X, Yang L, Nilsson-Payant BE, Wang P, Duan F, Tang X, Yaron TM, Zhang T, Uhl S, Bram Y, Richardson C, Zhu J, Zhao Z, Redmond D, Houghton S, Nguyen D-HT, Xu D, Wang X, Jessurun J, Borczuk A, Huang Y, Johnson JL, Liu Y, Xiang J, Wang H, Cantley LC, tenOever BR, Ho DD, Pan FC, et al. Identification of SARS-CoV-2 inhibitors using lung and colonic organoids. *Nature* 2021; 589: 270–275.
52. Youk J, Kim T, Evans KV, Jeong Y-I, Hur Y, Hong SP, Kim JH, Yi K, Kim SY, Na KJ, Bleazard T, Kim HM, Fellows M, Mahbubani KT, Saeb-Parsy K, Kim SY, Kim YT, Koh GY, Choi B-S, Ju YS, Lee J-H. Three-Dimensional Human Alveolar Stem Cell Culture Models Reveal Infection Response to SARS-CoV-2. *Cell Stem Cell* 2020; 27: 905-919.e10.
53. Salahudeen AA, Choi SS, Rustagi A, Zhu J, van Unen V, de la O SM, Flynn RA, Margalef-Català M, Santos AJM, Ju J, Batish A, Usui T, Zheng GXY, Edwards CE, Wagar LE, Luca V, Anchang B, Nagendran M, Nguyen K, Hart DJ, Terry JM, Belgrader P, Ziraldo SB, Mikkelsen TS, Harbury PB, Glenn JS, Garcia KC, Davis MM, Baric RS, Sabatti C, et al. Progenitor identification and SARS-CoV-2 infection in human distal lung organoids. *Nature* 2020; 588: 670–675.
54. Co JY, Margalef-Català M, Monack DM, Amieva MR. Controlling the polarity of human gastrointestinal organoids to investigate epithelial biology and infectious diseases. *Nat Protoc* Nature Publishing Group; 2021; 16: 5171–5192.
55. Iakobachvili N, Leon-Icaza SA, Knoops K, Sachs N, Mazères S, Simeone R, Peixoto A, Bernard C, Murris-Espin M, Mazières J, Cam K, Chalut C, Guilhot C, López-Iglesias C, Ravelli RBG, Neyrolles O, Meunier E, Lugo-Villarino G, Clevers H, Cougoule C, Peters PJ. Mycobacteria–host interactions in human bronchiolar airway organoids. *Molecular Microbiology* 2022; 117: 682–692.
56. Lamers MM, Beumer J, van der Vaart J, Knoops K, Puschhof J, Breugem TI, Ravelli RBG, Paul van Schayck J, Mykytyn AZ, Duimel HQ, van Donselaar E, Riesebosch S, Kuijpers HJH, Schipper D, van de Wetering WJ, de Graaf M, Koopmans M, Cuppen E, Peters PJ, Haagmans BL, Clevers H. SARS-CoV-2 productively infects human gut enterocytes. *Science* 2020; 369: 50–54.
57. Veerati PC, Troy NM, Reid AT, Li NF, Nichol KS, Kaur P, Maltby S, Wark PAB, Knight DA, Bosco A, Grainge CL, Bartlett NW. Airway Epithelial Cell Immunity Is Delayed During Rhinovirus Infection in Asthma and COPD. *Front Immunol* 2020; 11: 974.

Figures

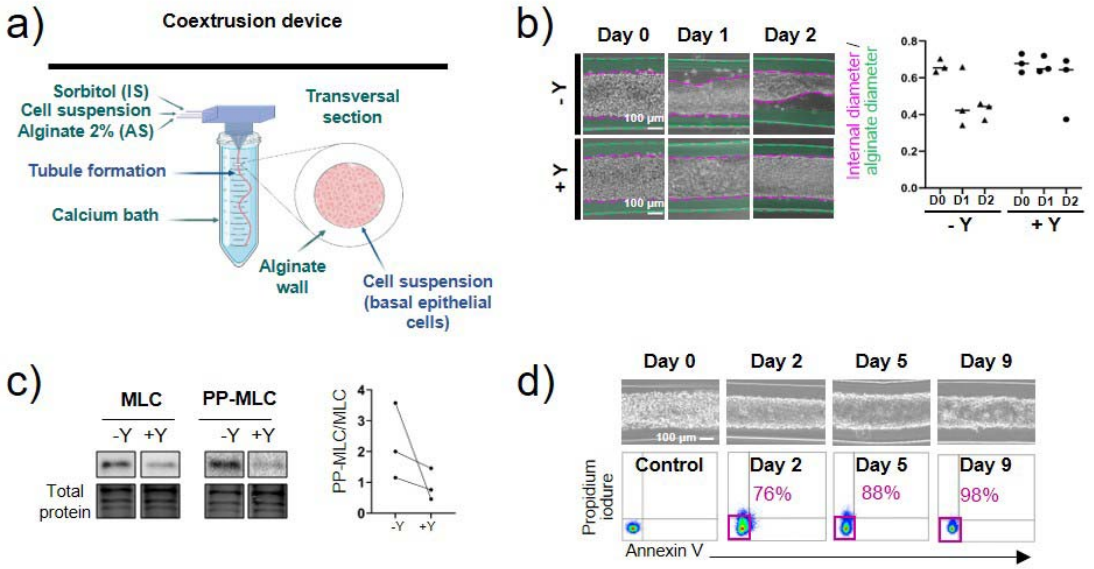

Figure 1. Formation of the alginate tube filled with primary basal epithelial cells, called "bronchioid". a) Schematic of the device to generate bronchioids. The three solutions are injected simultaneously by a computer-controlled pump, inside a 3D printed device soaked in a 100 mM calcium bath. b) Left panel: brightfield images of bronchioids over time, with or without (w/o) 10 µM Y-27632 ("Y"). Green and pink dotted lines indicate the external (alginate tube) and internal (epithelial tube) limits, respectively. Right panel: quantification of external and internal diameters (at least 10 measurements along the same tube for each condition, n=3 experiments). Medians are represented as horizontal lines. c) Immunoblots and analysis of myosin light chain (MLC) II and double-phospho-MLC (Thr18, Ser19; PP-MLC) expressions at day 2 on bronchioids from 3 different donors (i.e. n=3). Total protein stain was loading control. d) Upper panels: brightfield images of bronchioids cultured with 10 µM Y-27632. Lower panels: dot plots showing Propidium iodure (PI) fluorescence (y-axis) versus Annexin V- Allophycocyanin (APC) fluorescence (x-axis) in cells dissociated from bronchioids and analyzed by flow cytometry at indicated time points. Percentages of PI^- $Annexin\ V^-$ cells are shown in pink.

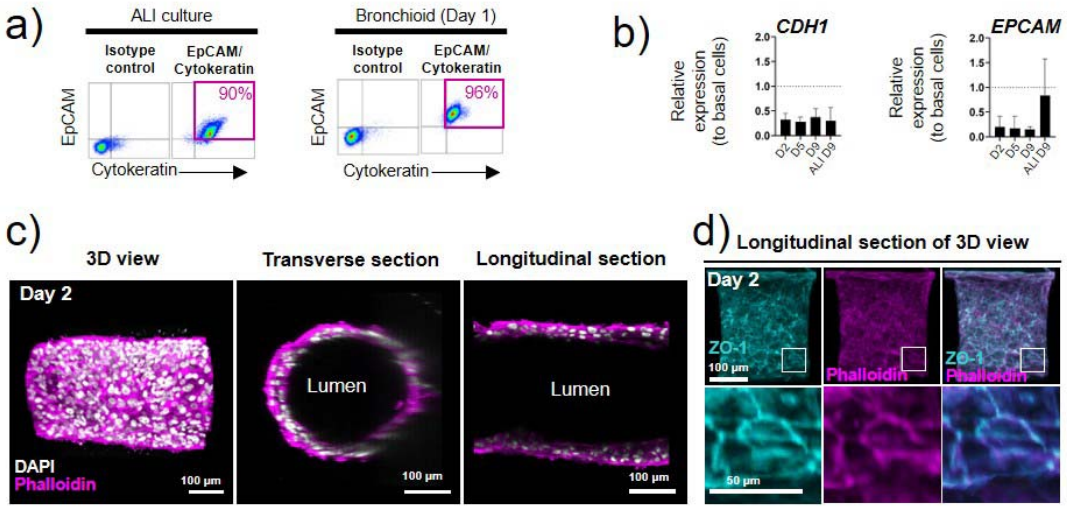

Figure 2. Characterization of the epithelial nature of cells in the the bronchioid model. a) Dot plots represent EpCAM-PerCP-Cy5.5 fluorescence (y-axis) versus pan cytokeratin-FITC fluorescence (x-axis) of cells dissociated from 2D air-liquid interface (ALI) culture and bronchioids at day 1. Gating strategy is shown in the left panels. Percentages of EpCAM^{+} cytokeratin^{+} cells are shown in pink. b) Expression of genes *CDH1* and *EPCAM* in bronchioids over time, and in cells dissociated from 2D culture after 9 days after ALI introduction. The samples are from 6 and 3 different donors for bronchioids and ALI culture, respectively (mean ± standard deviation, n=6 and n=3). Gene expression was normalized to the housekeeping genes *PPIA*, *RPL13* and *GusB* and expressed relative to basal epithelial cells in 2D submerged culture. c-d) Longitudinal, transversal sections and 3D views of 3D reconstructions obtained from Z-stack confocal images of 2-day-old stained for F-actin (phalloidin, magenta) and nucleus (DAPI, white) (c), for F-actin (magenta), ZO-1 (cyan) and nucleus (white) (d).

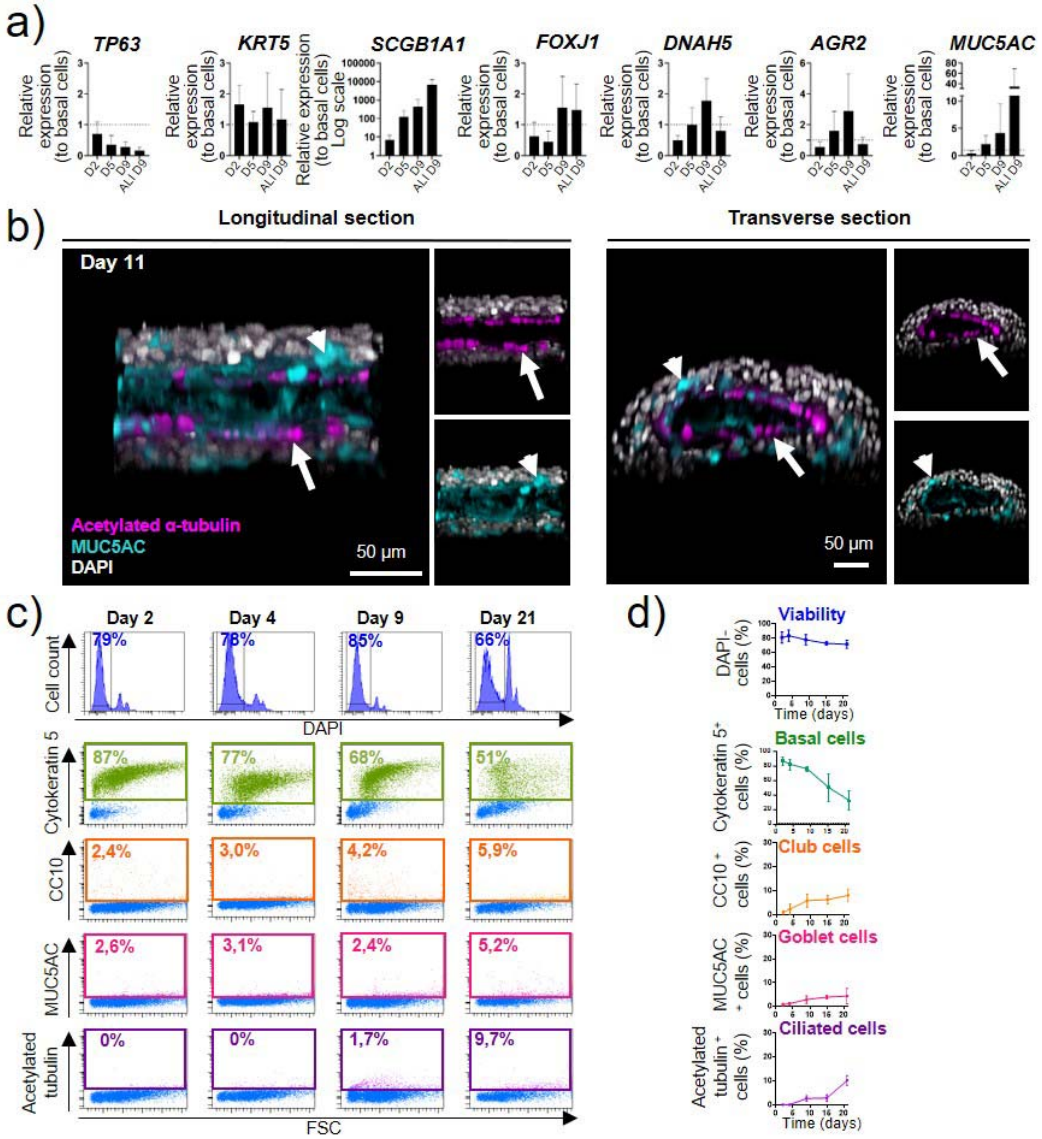

Figure 3. Differentiation induction of primary bronchial epithelial cells into bronchioids. a) Expression of genes *TP63*, *KRT5*, *SCGB1A1*, *FOXJ1*, *DNAH5*, *AGR2* and *MUC5AC* in bronchioids over time, and in cells dissociated from 2D culture after 9 days after ALI introduction. The samples are from 6 and 3 different donors for bronchioids and ALI culture, respectively (mean ± standard deviation, n=6 and n=3). Gene expression was normalized to the housekeeping genes *PPIA*, *RPL13* and *GusB* and expressed relative to basal epithelial cells in 2D submerged culture. b) Longitudinal, transversal sections and 3D views of 3D reconstructions obtained from z-stack confocal images of 11-day-old bronchioid stained for

acetylated α-tubulin (magenta), MUC5AC (cyan) and nucleus (white). Arrows: ciliated cells; arrowheads: goblet cells. c) Histograms represent representative cell count (y-axis) versus DAPI fluorescence (x-axis) of cells dissociated from bronchioids at indicated time points. Dot plots represent representative keratin-5/CC10/MUC5AC/acetylated tubulin fluorescence (y-axis) versus forward side scatted (FSC, x-axis). $DAPI^-$, cytokeratin 5^+ cells, $CC10^+$ cells, $MUC5AC^+$ cells, and acetylated $tubulin^+$ cells are shown respectively in dark blue, green, orange, pink and purple. d) Percentages of $DAPI^-$ cells, cytokeratin 5^+ cells, $CC10^+$ cells, $MUC5AC^+$ cells, and acetylated $tubulin^+$ cells over time. The samples are from 4 different non-COPD donors (i.e. n=4).

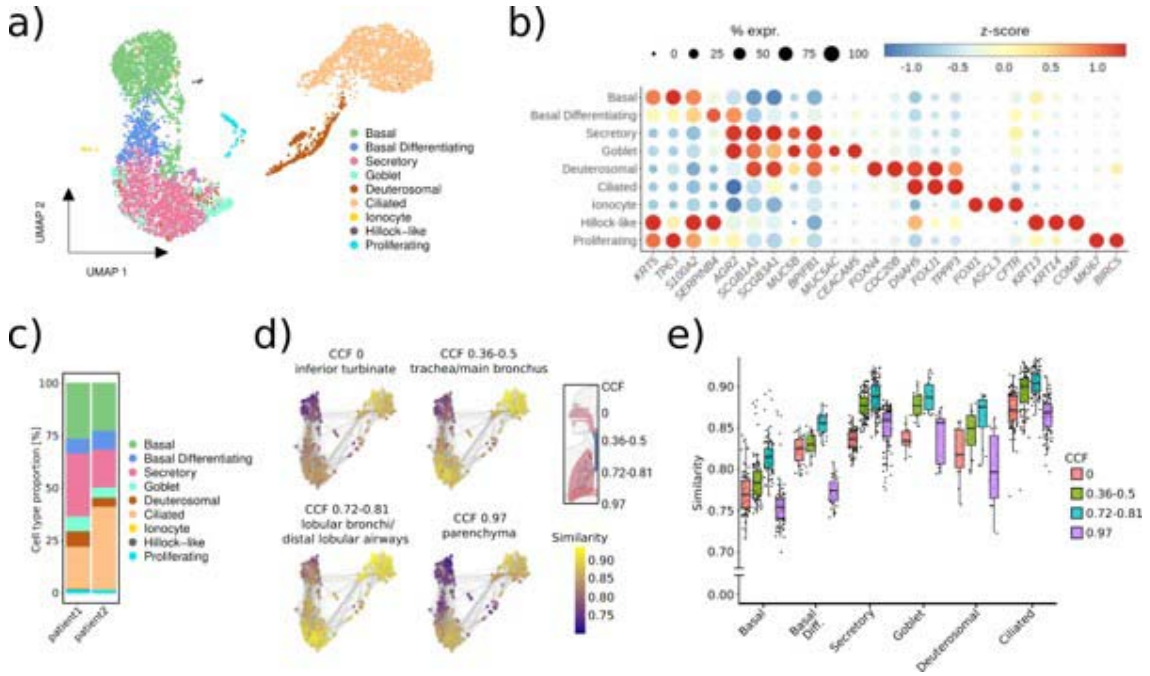

Figure 4. Single-cell transcriptome profiling in the bronchioid model. a) UMAP representation of scRNA-seq transcriptomic data showing the different cell types detected in 21-day-old bronchioids from 2 different non-COPD donors (i.e. n=2, patients 1 and 2). b) Dot plot showing scaled mean expression (color) and percentage of expressing cells (dot size) of selected marker genes in indicated cell groups c) Relative abundance of cell types identified in bronchioids from patients 1 and 2. d) Bronchioid neighbourhoods, positioned with respect to the UMAP embedding of each index cell, are coloured by the maximum correlation value across primary lung tissue neighborhoods from 4 distinct anatomical locations based on the common coordinate framework (CCF) established in the HLCA [30]. e) Box plot depicting neighborhood similarities of bronchioid neighborhoods with primary lung tissue neighborhoods in the respective CCF category over major cell types identifed in the bronchioid scRNA-seq data. Center line indicates the median, box limits indicate the upper and lower quantiles, and whiskers indicate the 1.5x interquartile range. In d–e, the bronchioid neighbourhoods were constructed from cells integrated across the 2 samples (n=2).

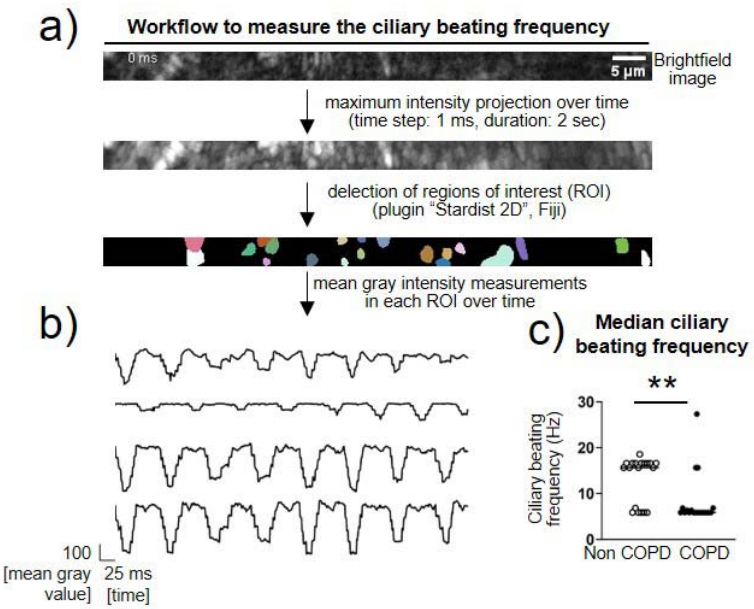

Figure 5. Fast Fourier transform (FFT) analysis of ciliary movement using high-speed video microscopy analysis. a) Schematic workflow to measure the ciliary beat frequency. Representative brightfield image corresponding to a part of a bronchioid at day 20. The coloured areas correspond to the regions of interest determined by the plugin "Stardist 2D" of the Fiji software on the image generated by a maximum intensity projection over time. b) Representative measurements of the mean intensity in regions of interest over time. The main frequency is determined using fast Fourier transform in each region of interest. c) Quantification of ciliary beat frequency (CBF) measurement in Hertz (Hz) of bronchioids derived from 4 different patients (n=2 non-COPD patients, n=2 COPD patients). For each patient, individual values represent median CBF, determined in 9-10 fields. Medians are represented as horizontal lines. **: P <0.01, Mann-Whitney test.

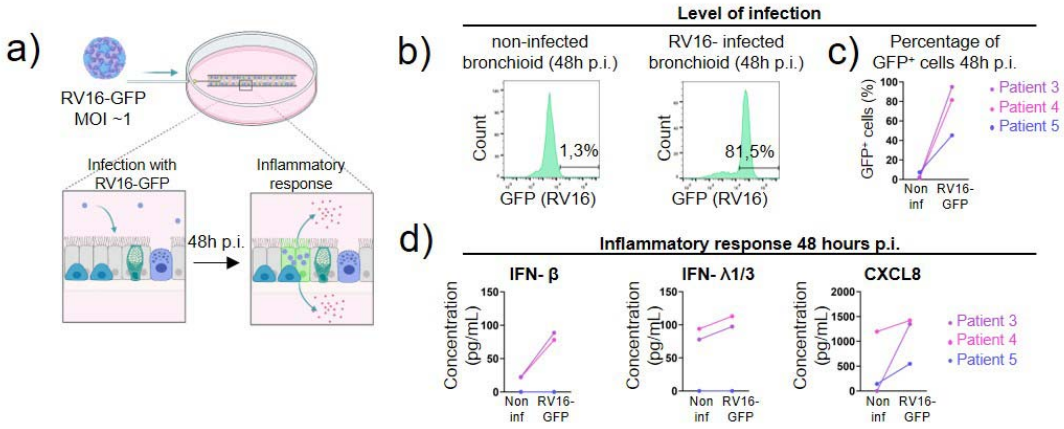

Figure 6. Rhinovirus infection in the bronchioid model. a) Experimental design to test rhinovirus type 16-green fluorescent protein (RV16-GFP) infection. Multiplicity of infection (MOI). b**)** Histograms represent representative cell count (y-axis) versus GFP fluorescence (x-axis) in the different conditions 48h post-infection. The percentages indicate the level GFP positive cells. c) Percentages of GFP^+ cells 48h post-infection, in bronchioids from 3 different donors (i.e. n=3, patients 1, 2 and 3)., in non-infected ("non inf") and infected ("RV16-GFP") conditions. d) IFN-β, IFN-λ1/3 and CXCL8 concentrations in the medium from bronchioid cultures in the different conditions.

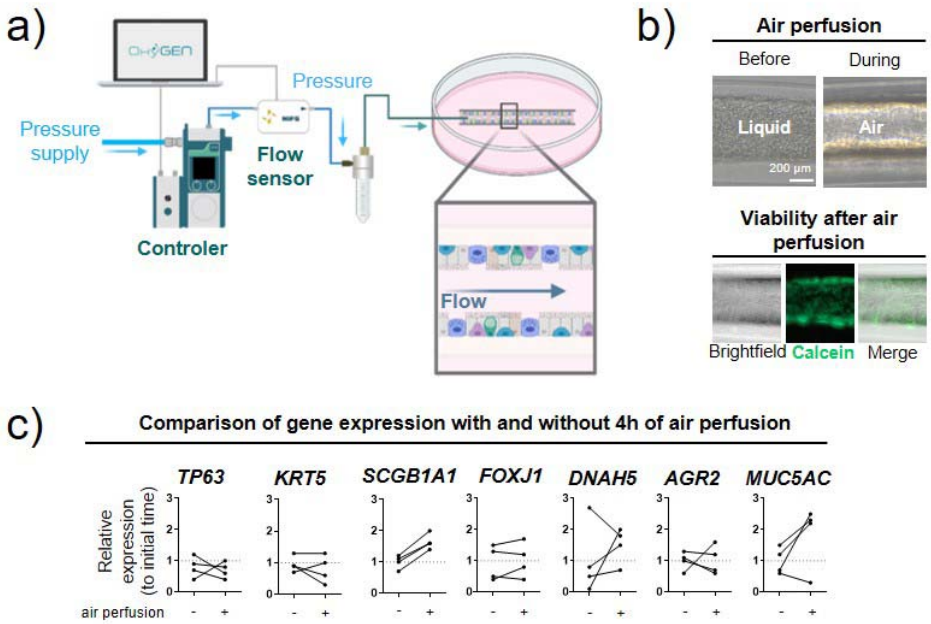

Figure 7. Establishment of an air-liquid interface in the bronchioid model. a) Set up for air perfusion. b) Upper panel: brightfield images of bronchioid before and during air perfusion. Lower panel: brightfield and fluorescence images of bronchioid after 4h perfusion and calcein staining. c) Comparison of gene expresssion (*TP63*, *KRT5*, *SCGB1A1*, *FOXJ1*, *DNAH5*, *AGR2*, *MUC5AC)* in bronchioids with and without 4h of perfusion, from 4 different non-COPD donors (mean ± standard deviation, n=4). Gene expression was normalized to the housekeeping genes *PPIA*, *RPL13* and *GusB* and expressed relative to bronchioids before perfusion (initial time).

Supplemental material

Supplemental material includes Tables E1, E2 and E2, figures E1 to E4, movies E1, E2 and E3.

Table 1: Patient characteristics for bronchioid generation

	Non-COPD patients	COPD patients
n	18	10
Age (years)	67.3 ± 8.6	66.6 ± 6.1
Sex (Men/Woman)	8/10	5/5
Current /Former/Non smokers	4/10/4	2/7/0*
Pack years (no.)	33.9 ± 12.6	48.9 ± 32.7*
PFT		
FEV1 (% pred.)	90.9± 29.6*	77.3 ± 11.4
FEV1/FVC ratio (%)	76,0± 10.8**	66.5 ± 4.5*

Plus–minus values are means ± SD. PFT, pulmonary function test; FEV_1, forced expiratory volume in 1 second; FVC, forced vital capacity. * one missing value ** two missing values. Even if the value of FEV1/FVC is not available here, COPD has been previously diagnosed by a physician.